ARTICLES

Dynamics of the CH($A^2\Delta$) Product from the Reaction of C_2H with O_2 Studied by Fourier Transform Visible Spectroscopy

Alan N. Arrowsmith,[†,‡] Viktor Chikan,[‡,§] and Stephen R. Leone*[,‡]

JILA, National Institute of Standards and Technology and Department of Chemistry and Biochemistry, University of Colorado, Boulder, Colorado 80309, Departments of Chemistry and Physics and Lawrence Berkeley National Laboratory, University of California, Berkeley, California 94720

Received: February 27, 2006; In Final Form: April 18, 2006

The reaction $C_2H + O_2 \rightarrow CH(A^2\Delta) + CO_2$ is investigated using Fourier transform visible emission spectroscopy. C_2H radicals, produced by 193 nm photolysis of C_2H_2, react with O_2 molecules at low total pressures to produce electronically excited CH($A^2\Delta$). Observation of the CH($A^2\Delta-X^2\Pi$) electronic emission to infer nascent rotational and vibrational CH($A^2\Delta$) distributions provides information about energy partitioning in the CH($A^2\Delta$) fragment during the reaction. The rotational and vibrational populations of the CH($A^2\Delta$) product are determined by fitting the rotationally resolved experimental spectra with simulated spectra. The CH($A^2\Delta$) product is found to be rotationally and vibrationally excited with $T_{rot} \cong 1150$ K and $T_{vib} \cong 1900$ K. The mechanism for this reaction proceeds through one of two five-atom intermediates and requires a crossing between electronic potential surfaces. The rotational excitation suggests a bent geometry for the final intermediate of this reaction before dissociation to products, and the vibrational excitation involves an elongation of the C−H bond from the compressed transition state to the final CH(A) state.

Introduction

In 1961, Bass and Broida attributed the intense blue emission observed in hydrocarbon flames at $\lambda \cong 430$ nm to the CH($A^2\Delta-X^2\Pi$) electronic transition.[1] Since then, several different mechanisms to explain the formation of CH($A^2\Delta$) (henceforth denoted CH*) in flames have been proposed.[2−8] Numerous studies have been carried out to test the validity of these proposals,[7−11] and attempts have been made to determine the specific chemical process(es) responsible for CH* formation in hydrocarbon flames. Given the complex nature of the chemical environments produced in hydrocarbon flames, as well as the widely variable conditions under which combustion can occur, it is not surprising that these processes have not yet been completely elucidated.

Gaydon first proposed a mechanism suggesting that the CH* emission is due to the $C_2 + OH \rightarrow CH + CO$ reaction.[3,4] This proposed mechanism was supported by the observation that the [CH*]/([C_2][OH]) ratio in hydrocarbon flames is independent of several flame parameters, namely, the concentration of an inert diluent, the fuel to oxidizer mixture, the reactant flow rate, and the measurement height above the burner.[12] Brenig et al. rejected the above mechanism, showing that no CH* is observed in systems containing C_2 and OH when O atoms are not present.[13] Several groups[2,5,6,14] suggested that the O atoms play an essential role in the formation of CH*, which can be attributed to one important mechanism:

$$C_2H + O \rightarrow CH^* + CO \quad \Delta H_f^\circ{}_{298} = -11 \text{ kcal/mol } (-46 \text{ kJ/mol}) + \text{other channels} \quad \text{(r1)}$$

The ethynyl radical can also react with molecular oxygen to form CH*, as first suggested by Renlund et al.[7,8]

$$C_2H + O_2 \rightarrow CH^* + CO_2 \quad \Delta H_f^\circ{}_{298} = -19 \text{ kcal/mol } (-80 \text{ kJ/mol}) + \text{other channels} \quad \text{(r2)}$$

Both of these reactions have been verified experimentally[6,7] to produce CH*. The room-temperature rate constants of (r1) and (r2) have been measured and are found to be 1.8×10^{-11} and 3.6×10^{-14} cm^3·molecule^{-1}·s^{-1}, respectively.[6] The overall rate constant for the reaction of C_2H with O_2 is 3.2×10^{-11} cm^3·molecule^{-1}·s^{-1}.[15] Although the rate coefficient of (r1) is 500 times greater than that of (r2), the importance of the reaction of C_2H with O_2 cannot be discounted in typical flame conditions. Experimental and theoretical work by Norton and Smythe shows that in a standard pressure CH_4/air flame, [O_2] is more than 500 times that of [O] in at least one-third of the flame area at the measured height (∼9 mm) above the burner.[16] Because the ratio of [O_2]/[O] ranges from ∼10 to ∼1000 in the flame, both (r1) and (r2) can contribute significantly to the production of CH*. Another recent study of the temperature dependence of the rate constant for (r2) also suggests that (r2) is a significant source of CH* in hydrocarbon flames and probably the dominant source relative to (r1) under fuel-lean conditions.[17]

In this paper we investigate the dynamics of CH* produced in reaction r2 by measuring the nascent rotational and vibrational energy distribution of the CH* product. C_2H radical, produced

[†] University of Colorado.
[‡] University of California.
[§] Current address: Department of Chemistry, Kansas State University, Manhattan, KS 66506.

10.1021/jp061246e CCC: $33.50
Published on Web 05/25/2006

by photodissociation of C_2H_2, reacts with O_2 to form CH* with an exothermicity of $\Delta H_f^\circ{}_{298} = -19$ kcal/mol (-80 kJ/mol). The rotationally resolved CH* emission spectra from the $v',v'' =$ (0,0) and (1,1) electronic transitions are obtained via Fourier transform (FT) visible emission spectroscopy. The experimentally obtained spectra are fitted with simulated spectra, allowing extraction of the rotational and vibrational populations of the CH* product. Further tests show that nascent population distributions can be obtained. The results indicate a vibrationally and rotationally excited CH* product: the vibrational temperature ($v' = 1/v' = 0$) is 1900 $\pm$ 250 K and the rotational temperatures for the $v' = 0$ and $v' = 1$ vibrational levels are 1150 $\pm$ 50 and 1100 $\pm$ 200 K, respectively. The considerable rotational excitation suggests a bent geometry for the final step in the reaction producing CH*. Because the reduced mass of the CH* fragment is small, the substantial vibrational excitation is most likely caused by a change in the C$-$H bond length in going from the transition state to the products, as opposed to energy imparted impulsively during the dissociation of the CH* fragment. These results are in agreement with anticipated theoretical transition states[18,19] for the ground state reaction $C_2H + O_2 \rightarrow CH(X) + CO_2$. However, no theoretical work has yet addressed the dynamical aspects of the formation of CH* via this reaction. The possible mechanisms for (r2), involving a number of intermediates as well as a crossing between electronic surfaces, are examined and evaluated with respect to the rotational and vibrational energy distribution in the CH* product.

Experimental Section

The experimental apparatus is documented in detail in previous publications[20,21] and only a brief description is given here. The experimental setup consists of a 193 nm ArF excimer laser, a vacuum chamber, and an FT-visible spectrometer. Oxygen and acetylene gases are mixed and introduced to the vacuum chamber through a 1 cm diameter stainless steel tube terminating $\sim$0.5 cm above the interaction region. The reactant gas flow intersects the excimer laser beam at right angles in the center of the vacuum chamber. The excimer laser beam is focused to a 1 cm^2 spot size at the interaction region. The energy density of the excimer laser beam is kept below 70 mJ$\cdot$pulse$^{-1}\cdot$cm^{-2} to minimize the possibility of multiphoton processes.[22] The repetition rate of the laser is set at 90 Hz. Argon is introduced into the chamber through multiple effusive openings near the windows, designed both to contain the reactant molecules within the interaction region and to keep the windows clean.

Radiation emitted from the interaction region is collected by a collimating lens at right angles to both the (vertical) gas flow and the (horizontal) excimer laser beam. A spherical mirror is placed opposite the collimating lens to increase the collection efficiency. The collimated light is then focused onto the entrance port of the step scan FT-visible spectrometer. Interferometric detection requires limiting the field of view[23] to enhance the spectral resolution of the FT-visible instrument. This is achieved by placing an iris (5 mm diameter) directly in front of the spectrometer entrance port. The iris also serves to reduce stray light admitted to the spectrometer. A blue sensitive photomultiplier tube (PMT) used in analogue mode detects the interferometric signal. The PMT signal is averaged using a boxcar integrator, gated from 5 to 15 μs after the excimer laser pulse. The gated signal is digitized and recorded by a computer. At each mirror position of the interferometer, the signal is coadded by summing over 200 laser pulses to increase the signal-to-noise ratio in the spectra. A total of 4096 data points (one point = one mirror position) is collected for each spectrum, spanning the spectral region from 22 120 to 23 700 cm^{-1}. The resulting experimentally limited spectral resolution is measured to be $\sim$0.8 cm^{-1}. The repetition rate of the excimer laser limits the data collection speed, so each spectrum takes approximately 2.5 h to collect. Ten such spectra collected as described above are averaged to obtain the final desired signal-to-noise ratio before fitting. Spectra are collected with 15 mTorr (2.0 Pa) C_2H_2 and 25 mTorr (3.3 Pa) O_2 in the reaction chamber, and the total pressure is varied from 100 mTorr (13.3 Pa) to 300 mTorr (40.0 Pa) by addition of Ar. The averaged spectra are multiplied by the measured instrument response function versus frequency for the spectrometer to obtain the actual spectra. The instrument response function is determined by measuring the emission from a known calibration lamp under circumstances identical to those of the experiment.

C_2H radicals are generated by 193 nm photolysis of acetylene (99.6%), which is purified by an activated carbon trap to remove the residual acetone stabilizer from the acetylene reagent flow. The trap is evacuated overnight before each experiment to ensure efficient removal of acetone. Pressures are measured using capacitance manometers. The gas flows are regulated by needle valves and measured by standard mass flow meters. The overall pressure in the chamber is controlled by varying the flow of Ar into the chamber.

Measurements of the CH* emission intensity versus laser pulse power density are obtained by taking the collimated emission from the chamber through a 430 $\pm$ 10 nm interference filter and focusing it onto a PMT, as opposed to focusing directly into the spectrometer entrance port. As a test for acetone contamination (see Results), a separate measurement of CH* emission intensity versus laser pulse power density from acetone photodissociation is performed by introducing acetone vapor mixed with air at room temperature into the reaction chamber at very low pressures ($\sim$1 mTorr (0.13 Pa)).

Results

In this study the CH* product of the $C_2H + O_2$ reaction is observed via rotationally resolved FT-visible spectroscopy. The C_2H radicals are formed by 193 nm excimer laser photodissociation of C_2H_2 molecules.[24$-$26] Figure 1 shows the signals of CH* emission intensity vs time produced by the photolysis of C_2H_2 in the presence (trace a), and in the absence (trace b), of O_2. These signals were obtained by placing a PMT directly after the reaction chamber and collecting the emitted light without passing the emission through the spectrometer. A 430 $\pm$ 10 nm interference filter placed in front of the PMT removes any light that is not produced by CH* emission. Low resolution spectra of the signals, gated from -2.5 to 2.5 μs and from 5 to 15 μs, confirm that the signals are indeed due to CH* emission. The prompt ($t < 2.5$ μs) CH* signal is present when C_2H_2 is photolyzed both in the presence (trace a) and in the absence (trace b) of O_2. However, the later time ($t > 2.5$ μs) CH* signal is present only when C_2H_2 is photolyzed in the presence of O_2. The later time signal in trace 1a is attributed to CH* produced from the reaction of C_2H with O_2. The decay constant of the later portion of this signal (9.6 μs) is in agreement with the expected C_2H removal rate. Contribution to this signal from the reaction of C_2H with $O(^3P)$ is negligible due to the extremely low 193 nm O_2 absorption cross section of 7×10^{-23} cm^2.[27]

Because acetone is present in the C_2H_2 cylinder as a stabilizer, we considered the possibility that acetone could account for the initial CH* emission signal. In an attempt to identify the source of the prompt CH*, we measured the dependence of the initial CH* emission intensity on the photolysis laser power

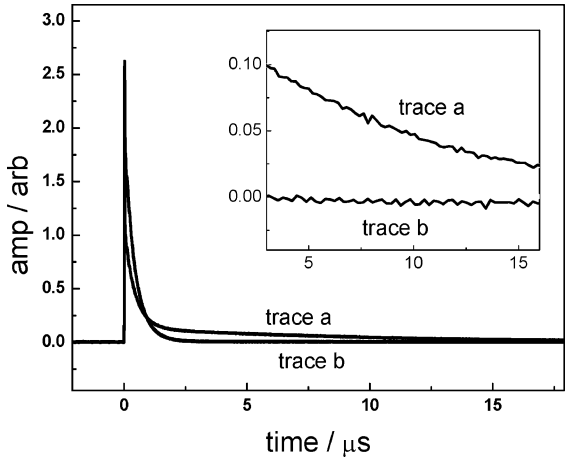

Figure 1. CH* emission intensity vs time (t_0 is initiated by the excimer laser pulse). Trace a shows the signal obtained with 15 mTorr (2.0 Pa) C_2H_2 and 25 mTorr (3.3 Pa) O_2 in the reaction chamber. Trace b shows the signal obtained with 15 mTorr (2.0 Pa) C_2H_2 and no O_2 in the reaction chamber. In both cases the total pressure in the reaction chamber is brought to 150 mTorr (20.0 Pa) by addition of Ar. The laser energy density is 60 mJ·pulse^{-1}·cm^{-2}. The signals are collected through a 430 ± 10 nm interference filter. The inset shows an expansion of the 5−15 μs time slice that is averaged to collect data in this experiment. The vertical axis scale of the inset is the same as the main figure axis scale.

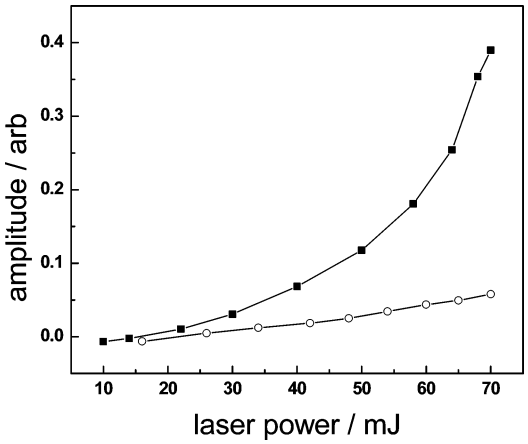

Figure 2. CH* emission intensity vs photolysis laser power for C_2H_2 photolysis (○) and acetone photolysis (■). CH* from C_2H_2 photolysis exhibits a linear dependence on laser power, whereas CH* from acetone photolysis exhibits a nearly cubic dependence. Measurements are taken with 15 mTorr (2.0 Pa) C_2H_2 or 1 mTorr (0.1 Pa) acetone in the reaction chamber, with a total pressure of 150 mTorr (20.0 Pa) obtained by addition of Ar.

for both the C_2H_2 used in the experiment and a separate sample of acetone. The dependence of the CH* emission signal on laser power is linear for C_2H_2 and nearly cubic for acetone. This result, shown in Figure 2, rules out acetone contamination as a source of the prompt CH* in Figure 1 because the two dependencies differ significantly. The possible source for the prompt CH* can be multiphoton dissociation of C_2H_2. However, this process is expected to have a quadratic dependence on laser power[28] rather than the observed linear dependence seen in Figure 2. Furthermore, multiphoton dissociation of C_2H_2 to CH* is not expected to occur at powers below 100 mJ·pulse^{-1}·cm^{-2}. Nonetheless, on the basis of the fast (<25 ns, detector-limited) rise time and subsequent exponential decay of the signal in Figure 1, trace b, we believe that the prompt CH* is produced directly from the C_2H_2 reactant molecule by laser multiphoton dissociation. The decay constant of this signal is consistent with

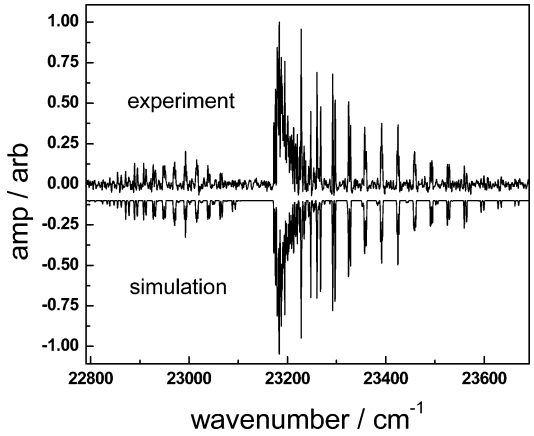

Figure 3. Experimental and simulated spectrum of CH* emission from the reaction $C_2H + O_2$. The data are taken with a high sensitivity photomultiplier tube at 0.8 cm^{-1} spectral resolution gated from 5 to 15 μs after the laser pulse. The total pressure is maintained at 150 mTorr (20.0 Pa) by addition of Ar; the C_2H_2 pressure is 15 mTorr (2.0 Pa), and the O_2 pressure is 25 mTorr (3.3 Pa). The laser fluence is 60 mJ·pulse^{-1}·cm^{-2}. The simulated spectrum is inverted for better visibility.

the CH* lifetime, implying that the CH* is only produced immediately with the laser pulse, and not subsequently. The higher power required for the multiphoton process could be due to a tightly focused "hot spot" in the laser pulse, and it is possible that the linear dependence over the power range examined is due to saturation of the CH* forming process. Fortunately, due to the short 537 ns CH* emission lifetime,[29] measurements taken at $t > 5$ μs will contain only a negligible contribution from the prompt CH*, as can be seen in the inset of Figure 1.

A rotationally resolved CH* emission spectrum, as well as its best fit simulated spectrum, are presented in Figure 3. The spectrum consists of three main branches (P, Q, and R), which are split by spin−orbit splitting and Λ doubling.[30] The separation due to Λ doubling is approximately 0.1 cm^{-1}, which cannot be resolved in this experiment. The spin−orbit splitting is easily observed in the P and R branches. The rotational populations are not affected by predissociation if the rotational quantum number N' is less than 23 for $v' = 0$ and less than 11 for $v' = 1$.[31]

The simulated spectrum is generated from the known molecular constants[32] and experimentally measured Einstein emission coefficients.[33] The rotational and vibrational populations are determined by minimizing the error (Er) between the experimental spectrum and the simulated spectrum according to

$$\mathrm{Er} = \sum_{j=\lambda_{\min}}^{\lambda_{\max}} [F_j \cdot g_j - f_j(p_i)]^2 \qquad (1)$$

In eq 1, F is the experimentally determined spectrum, f is the simulated spectrum as a function of p_i, g is the instrument response function, and the p_i are the vibrational populations and individual rotational populations of each vibrational level of CH*. The function f was constructed in a fashion similar to a computer program developed by Baas and Beenakker.[34]

CH* emission spectra from the reaction were collected at several total pressures in the reaction chamber varying from 100 mTorr (13.3 Pa) to 300 mTorr (40.0 Pa) to investigate the effect of total pressure on collisional relaxation of the CH* product, and to verify that the spectra collected at low total

TABLE 1: Rotational and Vibrational Temperatures of the CH* Product Derived from Experimental Results

pressure (mTorr (Pa))	$T_{rot}(v=0)$ (K)	$T_{rot}(v=1)$ (K)	T_{vib} (K)
100 (13.3)	1140 ± 60	1100 ± 200	2086 ± 250
150 (20.0)	1160 ± 50	1100 ± 500	1700 ± 250
200 (26.7)	1140 ± 60	890 ± 300	1850 ± 250
250 (33.3)	1120 ± 70	330 ± 70	1450 ± 250
300 (40.0)	1000 ± 50	200 ± 50	1850 ± 250

pressures represent nascent CH* emission. Rotational and vibrational temperatures derived from these spectra are shown in Table 1. The pressure is varied by altering the Ar pressure in the chamber while maintaining the same C_2H_2 and O_2 pressures. An attempt was made to vary the relative pressures of C_2H_2 and O_2, but any deviation from the optimum C_2H_2 and O_2 pressures resulted in a decrease of the signal-to-noise ratio such that spectra were no longer obtainable.

From Table 1, the spectra measured at a total pressure = 150 mTorr (20.0 Pa) represent the nascent distribution of CH* following the reaction r2. The nascent result is also reasonable on the basis of the following argument. If one assumes an average molecular speed of 700 m/s at a total pressure of 150 mTorr (20.0 Pa), the average time between collisions is ~2 μs. The emission lifetime of the CH(A) state (537 ns) is much shorter than the collision time; calculations show that the vast majority (>98%) of the emission from CH* at this pressure occurs prior to the CH* having suffered any collisions. Increasing the total pressure to 300 mTorr (40.0 Pa) decreases the calculated average time between collisions to ~0.7 μs, with the result that >30% of the CH* radicals suffer at least one collision before relaxation. Evidence for collisional relaxation of the CH* radical at a total pressure of 300 mTorr (40.0 Pa) can be seen in the experiments (Table 1). Measurements from 100 mTorr (13.3 Pa) to 250 mTorr (33.3 Pa) total pressure give a constant rotational temperature of ~1150 ± 50 K for the $v' = 0$ product, with a decrease to 1000 ± 50 K at 300 mTorr (40.0 Pa). The rotational temperature of the $v' = 1$ product shows a similar trend, although the temperature decrease begins at 250 mTorr (33.3 Pa) as opposed to 300 mTorr (40.0 Pa). It should be noted that the contribution of the (1,1) transition to the spectrum is only greater than the noise for the $j = 1-3$ peaks in the Q and R branches, and it is completely below the noise for the P branch; consequently, the error in the $v' = 1$ rotational temperatures is almost certainly significantly larger than the statistical errors quoted in Table 1.

Figure 4 shows a Boltzmann plot of the rotational populations vs energy for the (0,0) and (1,1) CH* electronic transitions. The rotational populations in this plot are derived from the CH* emission spectrum measured at 150 mTorr (20.0 Pa) total pressure, shown in Figure 3. This spectrum was chosen over the 100 mTorr (13.3 Pa) spectrum because of its superior signal-to-noise ratio, whereas the pressure is low enough to ensure that the measured spectrum comes from the nascent CH* on the basis of the above arguments. The plot indicates a rotational temperature of 1150 ± 50 K for the (0,0) transition and 1100 ± 200 K for the (1,1) transition of the CH* product. The observed vibrational temperature obtained by comparing the $v' = 1$ population to the $v' = 0$ population is 1900 ± 250 K.

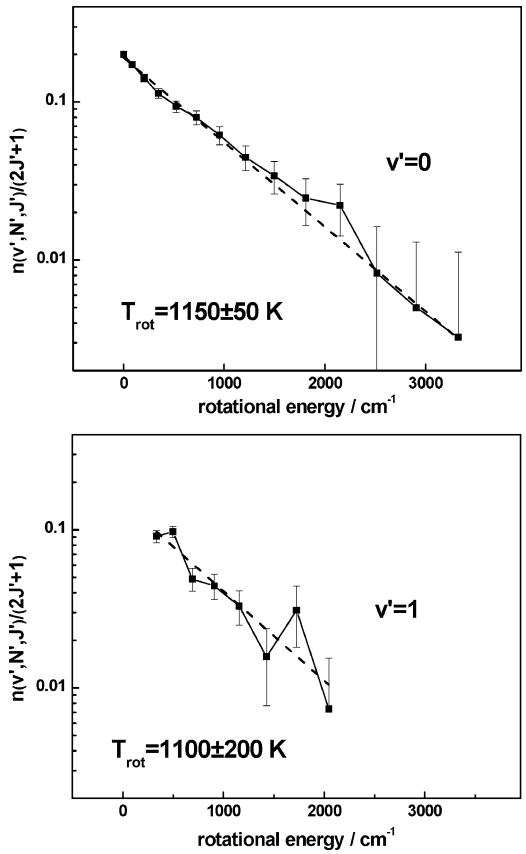

Figure 4. Experimentally determined nascent rotational distribution of CH* from $C_2H + O_2$ for $v' = 0$ and $v' = 1$. The dashed line indicates the fitting of the experimental nascent distribution with a Boltzmann distribution. The errors for the higher j population values in the $v' = 1$ plot may be larger than the errors shown, as discussed in the text. The rotational temperatures are found to be 1150 ± 50 K and 1100 ± 200 K. The vibrational temperature is 1900 ± 250 K.

Discussion

In this study the CH* product of the $C_2H + O_2$ reaction is observed via rotationally resolved FT-visible spectroscopy. Figure 1 shows traces of the signals resulting from CH* emission with and without O_2 present in the experiment. Given the fast rise time of the prompt signal in trace b, this prompt CH* is produced photolytically by the 193 nm laser pulse as discussed in the previous section. Regardless of the source of the prompt CH* observed from the photolysis of C_2H_2, it is clear from the inset in Figure 1 that CH* from this process is sufficiently relaxed by $t = 5$ μs that it contributes negligibly to the desired reaction signal. Therefore, CH* emission observed from the photolysis of C_2H_2 in the presence of O_2 after $t = 5$ μs is from a reaction of a C_2H_2 photolysis product with O_2. The only possible C_2H_2 photolysis products, other than an excited state of C_2H_2, are C_2H, CH, and C_2.[35] Of these species, only C_2H reacts with O_2 to form CH*. We are therefore confident that CH* observed after $t = 5$ μs in trace a of Figure 1 is produced by the reaction of C_2H with O_2.

Previous studies show that the 193 nm photolysis of C_2H_2 results in the production of $C_2H(\tilde{A})$ and $C_2H(\tilde{X})$ in the ratio ~ 1:9, with a significant proportion of the ground state C_2H in vibrationally excited states.[36] The actual observed fraction of CH* from the reaction of $C_2H(\tilde{A})$ or vibrationally excited $C_2H(\tilde{X})$ is probably much lower for several reasons. The exothermicity of the reaction ($C_2H(\tilde{A}) + O_2$) is about 4000 cm^{-1} greater than the reaction with ground state C_2H, which is enough energy to access higher vibrational states, such as CH* ($v = 2$), and even other electronic states, such as CH(B). No evidence for the presence of either of these states is observed in this experiment, and the higher vibrational states of CH* are predissociated.[31] On the basis of the relatively low rate constant for the reaction branch (r2), it also is less likely that reaction with vibrationally excited $C_2H(\tilde{X})$ occurs. The reason is that any initial HCCOO complex formed with significant vibrational

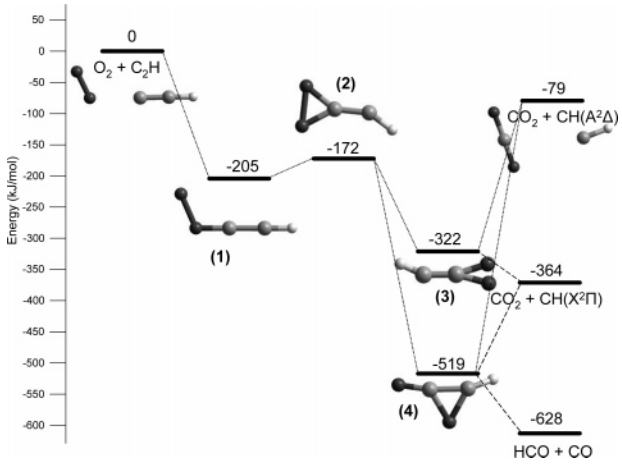

Figure 5. Simplified potential surface diagram showing relative energies and structures of intermediates for two proposed pathways of the $C_2H + O_2 \rightarrow CH^* + CO_2$ reaction (lines). Also shown are two other relevant product channels, producing $CH(X) + CO_2$ and HCO + CO (dashed lines). Numbers in parentheses are for identification; numbers without parentheses indicate relative energies of intermediates in kJ/mol. The figure is adapted from Sumathi et al.[18] Some transition state barriers may not be shown.

energy would redissociate to $C_2H + O_2$ rather than proceed to form the ring structure (2) of Figure 5, which is believed to be the rate-limiting step of the reaction.

Recent theoretical investigations of the $C_2H + O_2$ reaction have led to the proposal of two similar mechanisms to explain the formation of $CO_2 + CH$ on the ground state surface, shown in Figure 5.[18,19] Although these mechanisms do not account for the formation of CH*, a detailed examination of the mechanisms provides a groundwork from which to explore the formation of the electronically excited CH* product. The mechanisms differ in the configuration of the penultimate structures, (3) and (4) in Figure 5, as well as some variations in calculated bond lengths and angles. The following reaction mechanism is based on the work of Sumathi et al.[19] As mentioned above, the transition from structure (1) to (2) in Figure 5 is thought to be the rate-limiting step of the reaction, with a calculated transition state barrier height of ~20 kcal/mol (84 kJ/mol). Formation of structure (2) is supported by an analogous mechanism for the $C_2H_3 + O_2$ reaction, in which three-membered ring formation was shown to be favored over a four-membered ring.[37] Rearrangement to either structure (3) or (4) proceeds quickly through a much lower barrier (~4 kcal/mol (17 kJ/mol)). Dissociation of (3) should lead to $CO_2 + CH$ as the major channel, with energy imparted preferentially to CO_2 vibration and CH rotation (the calculated transition state HCC bond angle is 143°). Dissociation of (4) is thought to be dynamically controlled, leading predominantly to HCO + CO, with a small fraction undergoing vibrational redistribution to produce $CO_2 + CH$. In this case, the calculated transition state HCC bond angle is 124°, which might lead to slightly greater CH rotation compared to dissociation from (3). It should be noted that at present no theoretical treatment has specifically examined the production of $CO_2 + CH^*$, the electronically excited pathway. The CH* rotational and vibrational excitation measured in this experiment may be indicative of the geometry of the final intermediate of the reaction, either structure (3) or (4) of Figure 5. However, the electronically excited potential surface has to be accessed at some point along the reaction coordinate. There is no evidence from this experiment to suggest the location of the crossing. Fundamentally, the crossing could occur anywhere on the reaction coordinate. Without knowing the energetics of possible excited state intermediates, we can only make an educated guess based on the exothermicity of each step in the reaction as to where the crossing might occur. For the following analysis, we will assume that the crossing occurs during the final step of the reaction, as depicted in Figure 5 (other possibilities are considered briefly at the end of this section).

Table 1 shows the rotational temperatures for the $v' = 0$ and $v' = 1$ states of CH*, and the vibrational temperature obtained by comparing the $v' = 1$ to $v' = 0$ populations, at different total reaction pressures. As discussed above, the temperatures measured at 100 mTorr (13.3 Pa) and 150 mTorr (20.0 Pa) represent nascent CH* products, and the temperatures measured at higher pressures show effects of collisional relaxation of CH*. Because the (1,1) contribution to the emission spectrum is on the order of the noise level for $j > 3$, the $v' = 1$ rotational population assignments may contain a large error. Consequently, the $v' = 1$ rotational temperature and the vibrational temperature may have errors larger than the statistical errors quoted in Table 1. The resulting rotational temperature for the $v' = 0$ and $v' = 1$ states of 1150 ± 50 K is much higher than the room temperature thermal distribution, which indicates that rotational energy is imparted to the CH* fragment upon its dissociation. This can be consistent with both structures (3) and (4) of Figure 5 as an intermediate in the reaction, with calculated transition state HCC bond angles of 143° and 124° respectively, prior to the electronic surface crossing. The results of the experiments do not provide distinction between these two pathways. The lack of a bimodal rotational distribution suggests that the reaction may follow one or the other of these mechanisms predominantly, as opposed to being split between the two.

The $v' = 1/v' = 0$ vibrational temperature of the CH* product (1900 ± 250 K) is also much hotter than the rotational temperature distribution. Although this vibrational energy could be acquired impulsively by the CH* fragment as the HCCOO complex dissociates, the relatively low reduced mass of CH makes an impulsive transfer particularly inefficient. Alternatively, it is possible that this vibrational excitation is a result of a change in C−H bond length from the transition state to the products. The calculated C−H bond length in the ground transition state of structure (3) is 1.09 Å,[18] and that for structure (4) is 1.11 Å.[19] From spectroscopic constants,[32] the bond length of the CH* $v' = 0$ state is about 1.12 Å, and for the $v' = 1$ state about 1.15 Å. In this reaction, there would be a bond length increase of 0.03 Å from structure (3) or 0.01 Å from structure (4) going to $v' = 0$, and 0.06 Å from structure (3) or 0.04 Å from structure (4) going to $v' = 1$. Given the compressed structures in the transition states, one approach to interpret the vibrational dynamics may be to consider the overlap of the wave functions in the transition states and the CH* product. The compressed bond in the transition state may overlap better with the vibrational wave function of the $v' = 1$ state of CH* which has a smaller inner turning point of 0.95 Å compared to the $v' = 0$ state, with an inner turning point of 1.02 Å. Although this Franck−Condon-like approach is normally applied to fast processes, such as absorption of a photon, the concept may be extended to the time scale of a unimolecular dissociation reaction in the following way. Consider the potential surface for the C−H bond length along the reaction coordinate. It is possible that the reaction coordinate crosses a seam of intersection connecting the ground electronic potential surface with the electronically excited CH* surface, at which point the complex may undergo a surface crossing. In this picture the molecule approaches the transition state with a compressed C−H bond length but abruptly experiences a new potential after hopping to the new surface,

resulting in the observed vibrational excitation of the CH* fragment. If correct, this interpretation is supported by the observation of an even greater $v' = 1/v' = 0$ vibrational temperature (2800 K) for CH* produced by (r1).[38] In (r1), the final intermediate is the HCCO radical, which has a calculated C−H bond length in the transition state of 1.06−1.08 Å.[39−41] Thus, by this interpretation, the greater the required bond length increase, the larger the preferential population of the $v' = 1$ state. Impulsive vibrational energy transfer cannot be ruled out in either reaction. It should be noted that only ground state intermediates of (r2) have been tabulated for bond lengths in the transition state, but results for electronically excited intermediates (3) or (4) may have significantly different C−H bond lengths.

The crossing to an electronically excited potential surface to produce CH* is an important feature of this reaction mechanism and needs further theoretical input. The only certainty is that a crossing occurs somewhere in the mechanism, because the CH* product is observed. The mechanisms drawn in Figure 5 schematically depict the crossing during the final step of the reaction, and the above discussion of CH* product vibrational excitation also focuses on a crossing at this point. However, the highly exothermic step (2) → (3), (4) is another point at which the crossing could occur, in which case the transition state could already be on the appropriate electronic surface to produce CH*. It may prove revealing to search for an electronically excited analogue to structure (3) or (4), which could then dissociate to form CH*. Such a mechanism seems more plausible than a mechanism in which transfer of vibrational and rotational internal energy from (3) or (4) to the CH fragment is subsequently converted to electronic excitation. To our knowledge, no theoretical work has yet addressed the production of electronically excited CH* from this reaction.

Conclusion

The rovibrational product distribution of CH* from the reaction $C_2H + O_2 \rightarrow CH^* + CO_2$ was investigated using Fourier transform visible emission spectroscopy. The nascent rotational and vibrational populations of the CH* product were determined by fitting rotationally resolved experimental spectra to simulated spectra. The CH* product is found to be rotationally excited with $T_{rot} \cong 1150$ K. The vibrational temperature ($v' = 1/v' = 0$) is ∼1900 K. The mechanism for this reaction is complex and includes a crossing to an excited electronic potential. The rotational excitation suggests a bent geometry for the final intermediate of this reaction before dissociation to products, and the vibrational excitation suggests a C−H bond length change during the CH dissociation step. More theoretical work is required to understand the mechanism by which the electronically excited CH* product of this reaction is formed.

Acknowledgment. This work has been supported by the U.S. Department of Energy under the contract #DE-AC02-05CH11231. Personnel were also supported by the National Aeronautics and Space Administration and by the National Science Foundation.

References and Notes

(1) Bass, A. M.; Broida, H. P. *NBS Monogr.* **1961**, *24*.
(2) Brennen, W.; Carrington, T. *J. Chem. Phys.* **1967**, *46*, 7.
(3) Gaydon, A. G.; Wolfhard, H. G. *Flames*; Chapman and Hall: London, 1960.
(4) Gaydon, A. G. *The Spectroscopy of Flames*, 2nd ed.; Chapman and Hall: London, 1974.
(5) Devriendt, K.; Peeters, J. *J. Phys. Chem. A* **1997**, *101*, 2546.
(6) Devriendt, K.; VanLook, H.; Ceursters, B.; Peeters, J. *Chem. Phys. Lett.* **1996**, *261*, 450.
(7) Renlund, A. M.; Shokoohi, F.; Reisler, H.; Wittig, C. *Chem. Phys. Lett.* **1981**, *84*, 293.
(8) Renlund, A. M.; Shokoohi, F.; Reisler, H.; Wittig, C. *J. Phys. Chem.* **1982**, *86*, 4165.
(9) Lange, W.; Wagner, H. G. *Ber. Bunsen-Ges. Phys. Chem. Chem. Phys.* **1975**, *79*, 165.
(10) Laufer, A. H.; Lechleider, R. *J. Phys. Chem.* **1984**, *88*, 66.
(11) Lander, D. R.; Unfried, K. G.; Stephens, J. W.; Glass, G. P.; Curl, R. F. *J. Phys. Chem.* **1989**, *93*, 4109.
(12) Bulewicz, E. M.; Padley, P. J.; Smith, R. E. *Proceedings of the Royal Society of London Series a-Mathematical and Physical Sciences* **1970**, *315*, 129.
(13) Brenig, H. H. Ph.D. Thesis, Wuppertal, 1981.
(14) Glass, G. P.; Kistiakowsky, G. B.; Michael, J. V.; Niki, H. *Symp. (Int.) Combust. [Proc.]* **1965**, *10*, 513.
(15) Opansky, B. J.; Seakins, P. W.; Pedersen, J. O. P.; Leone, S. R. *J. Phys. Chem.* **1993**, *97*, 8583.
(16) Norton, T. S.; Smyth, K. C.; Miller, J. H.; Smooke, M. D. *Combust. Sci. Technol.* **1993**, *90*, 1.
(17) Elsamra, R. M. I.; Vranckx, S.; Carl, S. A. *J. Phys. Chem. A* **2005**, *109*, 10287.
(18) Li, L. C.; Deng, P.; Tian, A.; Xu, M. H.; Wong, N. B. *J. Phys. Chem. A* **2004**, *108*, 4428.
(19) Sumathi, R.; Peeters, J.; Nguyen, M. T. *Chem. Phys. Lett.* **1998**, *287*, 109.
(20) Chikan, V.; Nizamov, B.; Leone, S. R. *J. Phys. Chem. A* **2004**, *108*, 10770.
(21) Chikan, V.; Leone, S. R. *J. Phys. Chem. A* **2005**, *109*, 2525.
(22) Sorkhabi, O.; Blunt, V. M.; Lin, H.; Xu, D. D.; Wrobel, J.; Price, R.; Jackson, W. M. *J. Chem. Phys.* **1997**, *107*, 9842.
(23) Griffiths, P. R. *Fourier transform infrared spectrometry*; Wiley: New York, 1986.
(24) Shokoohi, F.; Watson, T. A.; Reisler, H.; Kong, F.; Renlund, A. M.; Wittig, C. *J. Phys. Chem.* **1986**, *90*, 5695.
(25) Wodtke, A. M.; Lee, Y. T. *J. Phys. Chem.* **1985**, *89*, 4744.
(26) Satyapal, S.; Bersohn, R. *J. Phys. Chem.* **1991**, *95*, 8004.
(27) Nicolet, M.; Cieslik, S.; Kennes, R. *Planet. Space Sci.* **1989**, *37*, 427.
(28) McDonald, J. R.; Baronavski, A. P.; Donnelly, V. M. *Chem. Phys.* **1978**, *33*, 161.
(29) Becker, K. H.; Brenig, H. H.; Tatarczyk, T. *Chemical Physics Lett.* **1980**, *71*, 242.
(30) Brazier, C. R.; Brown, J. M. *Can. J. Phys.* **1984**, *62*, 1563.
(31) Luque, J.; Crosley, D. R. *J. Chem. Phys.* **1996**, *104*, 2146.
(32) Zachwieja, M. *J. Mol. Spectrosc.* **1995**, *170*, 285.
(33) Luque, J.; Crosley, D. R. *SRI International Report No. MP 95-140*, 1995.
(34) Baas, R. C.; Beenakker, C. I. M. *Comput. Phys. Commun.* **1974**, *8*, 236.
(35) Campos, A.; Boye, S.; Brechignac, P.; Douin, S.; Fellows, C.; Shafizadeh, N.; Gauyacq, D. *Chem. Phys. Lett.* **1999**, *314*, 91.
(36) Hsu, Y. C.; Chen, F. T.; Chou, L. C.; Shiu, Y. J. *J. Chem. Phys.* **1996**, *105*, 9153.
(37) Mebel, A. M.; Diau, E. W. G.; Lin, M. C.; Morokuma, K. *J. Am. Chem. Soc.* **1996**, *118*, 9759.
(38) Chikan, V.; Leone, S. R. *J. Phys. Chem. A* **2005**, *109*, 10646. Chikan and Leone wish to note that the exothermicity of the $C_2H + O(^3P) \rightarrow C_2O + H$ is incorrect in this reference (187 kcal/mol was reported). The correct value is −71.5 kcal/mol. The paper ignores the possibility that a significant amount of $C_2O + H$ can form from the $C_2H + O$ reaction, because the $C_2O + H$ channel was not observed in a previous HCCO photodissociation experiment (*J. Chem. Phys.* **1996**, *105*, 6078.). The authors agree with the explanation provided in *J. Phys. Chem. A* **2005**, *109*, 10287, i.e., that the $C_2O + H$ channel can account for the difference between this work and a previous publication (*Chem. Phys. Lett.* **1996**, *261*, 450). More study is needed to confirm the presence of C_2O and to quantify the amount of C_2O from the $C_2H + O(^3P)$ reaction.
(39) Sattelmeyer, K. W.; Yamaguchi, Y.; Schaefer, H. F. *Chem. Phys. Lett.* **2004**, *383*, 266.
(40) Szalay, P. G.; Stanton, J. F.; Bartlett, R. J. *Chem. Phys. Lett.* **1992**, *193*, 573.
(41) Szalay, P. G.; Fogarasi, G.; Nemes, L. *Chem. Phys. Lett.* **1996**, *263*, 91.